I&EC research
Industrial & Engineering Chemistry Research
pubs.acs.org/IECR
Article

Rate-Based Absorption Modeling for Postcombustion CO_2 Capture with Additively Manufactured Structured Packing

Joshua A. Thompson* and Costas Tsouris

Cite This: *Ind. Eng. Chem. Res.* 2021, 60, 14845−14855
Read Online

ABSTRACT: Carbon capture using amine-based solvents in an absorption process is a leading candidate for reducing greenhouse gas emissions in industrial flue gas streams. To reduce operating costs and associated parasitic energy of these processes, process intensification utilizing additively manufactured structured packing has emerged as a new technology to manage exothermic reactions during absorption while improving CO_2 capture. A rate-based model framework has been developed for these novel packings that incorporates the mass and heat transfer phenomena for amine-based absorption of CO_2. The rate-based model framework is first benchmarked using available solubility data and pilot plant data for aqueous monoethanolamine. The model validation shows accurate prediction of both CO_2 equilibrium partial pressures and ion speciation for solubility data as well as CO_2 capture, temperature profile, and solvent composition for pilot plant data in the absorption column. The model framework is then applied toward predicting the CO_2 capture performance of additively manufactured structured packing. Simulations agree with experimental data in predicting the CO_2 capture and the capture performance increase due to cooling within the structured packing device. Advantages of this rate-based model framework are the utilization of correlations that may predict mass transfer and heat transfer coefficients of the packing based on the geometric properties of the device and the implementation of the model framework in open-source programming.

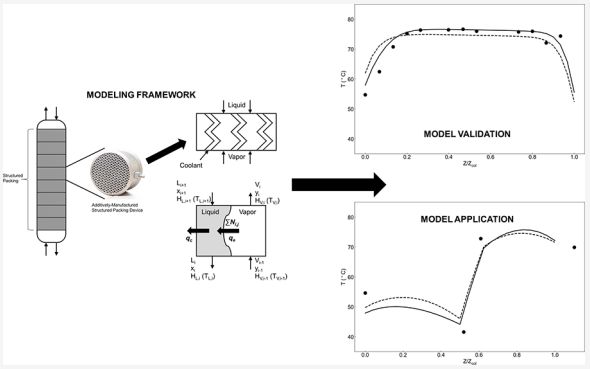

1. INTRODUCTION

Capture, utilization, and storage of carbon dioxide (CO_2) are necessary to reduce the impact of climate change from greenhouse gas emissions. Multiple technological approaches exist to reduce CO_2 emissions and its existing levels in the atmosphere through postcombustion capture, precombustion capture, oxyfuel combustion, and direct air capture.[1−5] Postcombustion capture is considered a near-term approach to achieve carbon neutrality in the industrial sector by removing CO_2 from existing and new flue gas streams. Methods of capture developed in chemical separations include absorption, adsorption, and membranes.[1,6−8] Among these technologies, absorption is considered the most mature, as it has been used extensively in industry for removing acidic gases from natural gas, hydrogen, and other industrial gas streams.[9]

Absorption utilizing amine chemistry to react CO_2 with the solvent has been investigated to demonstrate the capability of benchmark and novel solvents to scrub CO_2 from flue gas streams.[10−13] As absorption technology requires the regeneration of the solvent within a stripping column, research has focused on means of reducing the parasitic energy and capital investment of an amine-based process through innovative process configurations, solvent formulations, and their combinations.[12,14−16] This has led to studies of commercially available solvents, such as aqueous monoethanolamine (MEA), as well as the development of more advanced solvents, including novel amines, organic-based solvents, and ionic liquids.[13,16−20] A common difficulty in amine-based solvents for CO_2 capture is the management of the exothermic energy generated within the absorption column due to the reaction between CO_2 and the amine.[18,21,22] This phenomenon requires balance between the reaction kinetics, CO_2 solubility, and process design. Using aqueous MEA, there may be large temperature increases in the absorption column from absorption of CO_2, and utilization of heat exchangers between packed bed stages within an absorption column may be required to manage the exothermic reaction.[15,18,23]

Process improvements in absorption-based CO_2 capture have been achieved by either reducing the parasitic energy in regenerating the solvent or implementing new technology that enables process intensification for CO_2 capture. Reduction in the parasitic energy may be realized by utilizing a nonaqueous

Received: July 12, 2021
Revised: September 17, 2021
Accepted: September 20, 2021
Published: October 5, 2021

solvent with lower heat capacity compared to water or by utilizing the properties of the solvent to strip CO_2 at higher pressures with innovative heat integration in the process.[12,20,24,25] Rochelle and co-workers have achieved the latter using aqueous piperazine as the solvent and demonstrated the technology by both pilot plant campaigns and process simulations.[22,24,26] Process intensification may be achieved by reducing the size of the process equipment with an intensified or external field (e.g., high gravity rotation, microwaves) or by integrating multiple process units within one single piece of equipment (e.g., catalytic distillation).[27,28] Process intensification may lead to equipment size reduction by as much as 10-fold in volume in some cases.[28] For the process discussed here, the goal would be a 10−20% reduction in volume with an equivalent capital cost reduction for CO_2 capture plants.

Recently, an additively manufactured structured packing device was developed to demonstrate process intensification by utilizing printed heat exchangers incorporated in a packed bed used for mass transfer between flue gas and a solvent.[29−32] This concept combines the modularity of 3D printing prototypes with process integration concepts for interstage heat exchangers to improve the CO_2 capture rate of aqueous MEA.[32] An advantage of this technology is its use with any type of solvent for CO_2 capture. While scale-up of absorption-based process technology has been primarily evaluated through pilot plant campaigns coupled with modeling of these processes to estimate the cost to capture CO_2 from industrial gas streams, estimation of processes that may utilize additive manufacturing in CO_2 capture has been limited due to the complex heat and mass transfer and reaction between CO_2 and solvent that occur within an absorption column. However, recent work in developing mass transfer correlations and advances in open-source software tools may enable more rapid feedback in development of these prototypes to improve CO_2 capture performance and reduce manufacturing and operating costs.[33−36] Rochelle and co-workers have developed mass transfer correlations that only rely on geometric properties of structured packing, which are known and may be tailored through computer-aided design for additively manufactured packing devices.[35] Rate-based modeling relying on these mass transfer correlations is considered the most accurate method for estimating CO_2 capture performance of amine-based solvents and allows for use of a deterministic model to design and scale-up CO_2 capture processes.[18,37] These rate-based models may be performed by either an Enhancement factor-based model or by discretization of the liquid film and modeling the reaction kinetics more rigorously.[37,38]

A model framework that incorporates the complex heat and mass transfer within an additively manufactured structured packing device has been developed to estimate the improved performance of CO_2 capture using process intensification. This model framework is first validated with available CO_2 solubility data and published absorption column data from pilot plant campaigns ranging in scale and feed conditions for aqueous MEA. Different models for estimating the enhancement for mass transfer based on the reaction kinetics between CO_2 and MEA are compared to determine how simulations may be affected by these model assumptions. Comparison with these two different pilot plant studies will demonstrate how the framework here may be applicable to different column scales and column geometries in addition to other absorption column parameters that are often examined, such as CO_2 lean loadings, gas-to-liquid ratios, and amine concentrations. The CO_2 capture improvement utilizing additively manufactured structured packing is then simulated. Based on available correlations, both the CO_2 capture and temperature profile may be accurately predicted. This model framework may have further application in improving prototype and scale-up development of these novel structured packing devices for CO_2 capture.

2. MODEL FRAMEWORK

The model framework was developed based on previous rate-based, or nonequilibrium, modeling from Taylor and co-workers.[39,40] This previous modeling framework utilized a film model and Generalized Maxwell-Stefan relationships to describe the mass transfer within a packed or trayed column section and homogeneous reaction within the liquid-phase film. To simplify the model, the mass transfer flux was estimated by an Enhancement factor model rather than Maxwell-Stefan and homogeneous reaction relationships. The thermodynamic and chemical equilibria and transport and physical properties were calculated at each packed section. Details on equations and correlations in the model framework are provided in the Supporting Information. The model was developed within the Pyomo modeling language, using an interior point nonlinear solver (IPOPT).[41−43] The algorithm developed for this work first solved equations based on the feed conditions of the solvent and gas. The equations for mass transfer were then used to determine isothermal steady-state axial profiles in the absorption column. Adiabatic conditions in the column were then applied toward the energy balance equations to determine the initial steady state of the absorption column with both heat and mass transfer, and subsequent simulations that implemented cooling with the additively manufactured structured packing were solved based on these adiabatic results.

2.1. Chemical and Vapor−Liquid Equilibria. The following reactions may occur when CO_2 absorbs in aqueous MEA:

$$2H_2O \overset{K_1}{\leftrightarrow} OH^- + H_3O^+ \quad \text{(R1)}$$

$$CO_2 + 2H_2O \overset{K_2}{\leftrightarrow} HCO_3^- + H_3O^+ \quad \text{(R2)}$$

$$HCO_3^- + H_2O \overset{K_3}{\leftrightarrow} CO_3^{2-} + H_3O^+ \quad \text{(R3)}$$

$$MEAH^+ + H_2O \overset{K_4}{\leftrightarrow} MEA + H_3O^+ \quad \text{(R4)}$$

$$MEACOO^- + H_2O \overset{K_5}{\leftrightarrow} MEA + HCO_3^- \quad \text{(R5)}$$

The equilibrium reaction constants, K_i, were taken from correlations developed by Edwards et al. (K_1−K_3) and by Kent and Eisenberg (K_4 and K_5).[44,45] The mole and charge balances of ionic species are determined by

$$[MEA]_t = [MEA] + [MEAH^+] + [MEACOO^-] \quad (1)$$

$$[CO_2]_t = \alpha[MEA]_t = [CO_2] + [HCO_3^-] + [CO_3^{2-}] + [MEACOO^-] \quad (2)$$

$$[MEAH^+] + [H_3O^+] = [OH^-] + [HCO_3^-] + 2[CO_3^{2-}] + [MEACOO^-] \quad (3)$$

where α is the normalized loading for CO_2 in the solvent (mol CO_2/mol MEA). These coupled mole balances and equilibrium reactions determine the free CO_2 concentration in an

https://doi.org/10.1021/acs.iecr.1c02756
Ind. Eng. Chem. Res. 2021, 60, 14845−14855

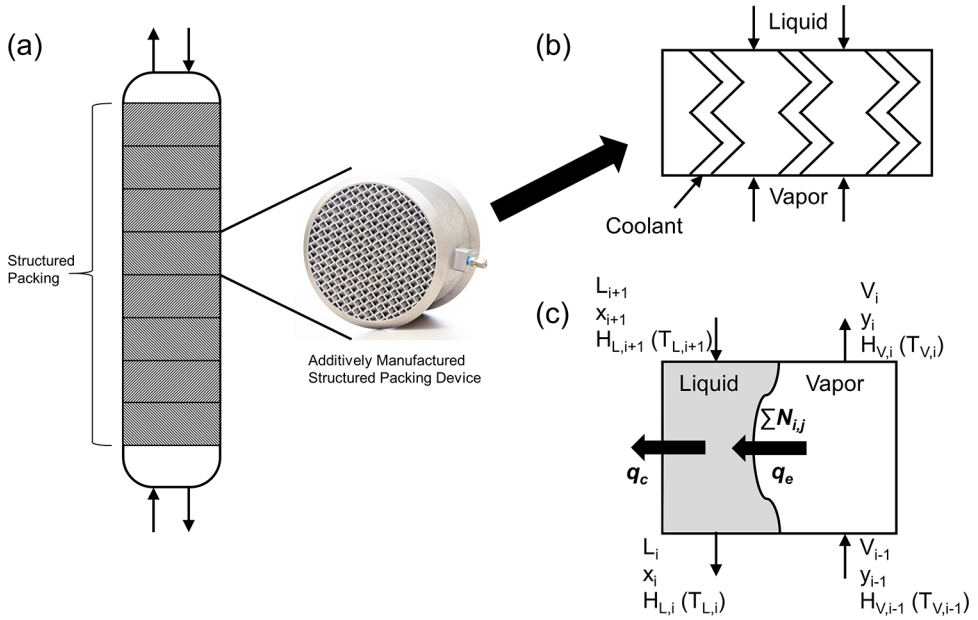

Figure 1. (a) Schematic representation of packed absorption column with individual packing sections and additively manufactured structured packing; (b) schematic of corrugated double-walled sheets that contain internal coolant channels and external mass transfer contacting area; and (c) film model representation of mass and energy balances of rate-based absorption with an additively manufactured device.

aqueous MEA solution, which may then be related to an equilibrium partial pressure for CO_2 by using the N_2O analogy[46]

$$y_{CO_2}\varphi_{CO_2}P = \gamma_{CO_2}[CO_2]H_{CO_2,w}\frac{H_{N_2O,MEA}}{H_{N_2O,w}} \tag{4}$$

where y is the mole fraction in the gas phase, φ is the gas-phase fugacity coefficient, P is the pressure, γ is the liquid-phase activity coefficient, H_i is Henry's constant for CO_2 and N_2O in either water or MEA, and $[CO_2]$ is the molar concentration of free CO_2. The equilibria for MEA and H_2O are determined by

$$y_{MEA}\varphi_{MEA}P = \gamma_{MEA}[MEA]P^s_{MEA} \tag{5a}$$

$$y_{H_2O}\varphi_{H_2O}P = a_w P^s_{H_2O} \tag{5b}$$

where P^s_i is the vapor pressure of component i, and a_w is the activity for water. The fugacity and activity coefficients may be described by equations of state, such as Soave–Redlich–Kwong, and electrolyte activity models, respectively.[47] For the modeling framework here, the gas phase is assumed to be ideal, such that φ_i is equal to unity for all gaseous components, and the activity coefficients for the ionic species are described by the Debye–Hückel equation

$$\ln \gamma_i = \frac{-z_i^2 A\sqrt{I}}{1 + 1.2\sqrt{I}} \tag{6}$$

where z_i is the charge of the component i, A is the Debye–Hückel law slope, and I is the ionic strength (mol/kg H_2O).[38,44] Activity coefficients for neutral species, CO_2 and MEA, are assumed to be unity, while the activity for water is

$$\ln a_w = MW_w\left(\frac{2AI^{3/2}}{1 + 1.2\sqrt{I}} - \sum_{i\neq w} m_i\right) \tag{7}$$

where MW_w is the molecular weight for water (kg/mol), and m_i is the molarity of component i (mol/kg).

2.2. Rate-Based Absorption. A schematic of a packed absorption column with additively manufactured structured packing and a representation of the rate-based absorption model framework are shown in Figure 1. The rate-based model represents a packed section, j, that is described by the following component and overall material balances[39,40]

$$y_{i,j}V_j - y_{i,j-1}V_{j-1} - N_{i,j} = 0 \tag{8a}$$

$$x_{i,j}L_j - x_{i,j+1}L_{j+1} + N_{i,j} = 0 \tag{8b}$$

$$L_j - L_{j+1} + V_j - V_{j-1} = 0 \tag{8c}$$

where y_i and x_i are the mole fractions of component i in the gas and liquid phases, respectively, and V and L are the gas and liquid molar flow rates, respectively, at stage j. The interfacial flux, $N_{i,j}$, is the mass transfer rate from the gas to the liquid phase for component i defined by

$$N_{i,j} = K_{i,OG}a_{e,j}A_j(y_{i,j}P_j - P^*_{i,j})\Delta z \tag{9}$$

where $a_{e,j}$ is the effective volume-specific interfacial area of the structured packing, P_j is the stage pressure, $P^*_{i,j}$ is the component equilibrium pressure at stage j, described by eqs 4 and 5, A_j is the column cross section area, and Δz is the discretized axial length of the column section. The overall, gas-side mass transfer coefficient, $K_{i,OG}$, is defined by

$$K_{CO_2,OG} = \left(\frac{RT_V}{k_{g,CO_2}} + \frac{H_{CO_2}}{Ek_{l,CO_2}}\right)^{-1} \tag{10a}$$

$$K_{i,OG} = \frac{k_{g,i}}{RT_V} \tag{10b}$$

where $k_{g,i}$ and $k_{l,i}$ are the gas- and liquid-side mass transfer coefficients of component i, H_{CO_2} is Henry's constant for CO_2 in aqueous MEA using the N_2O analogy, T_V is the gas-side temperature, R is the ideal gas constant, and E is the

https://doi.org/10.1021/acs.iecr.1c02756
Ind. Eng. Chem. Res. 2021, 60, 14845−14855

Enhancement factor due to chemical reaction between CO_2 and MEA. For components O_2 and N_2, the mass transfer flux, $N_{i,j}$, is assumed to be zero, such that no absorption into the solvent occurs, and the solubility, as a result, is assumed to be negligible.

The energy balances for the gas- and liquid-side are defined by

$$H_{V,j-1}V_{j-1} - H_{V,j}V_j - q_e = 0 \tag{11a}$$

$$H_{L,j+1}L_{j+1} - H_{L,j}L_j + q_e + \Delta H_{abs}N_{CO_2,j} + \sum_{i=MEA,W} \Delta H_{vap,i}N_{i,j} = 0 \tag{11b}$$

$$q_e = h_e a_{e,f} A_j (T_V - T_L)\Delta z \tag{11c}$$

where H_V and H_L are the molar enthalpy for the gas and liquid phases, respectively, q_e is the interfacial heat transfer between the gas and liquid phases, ΔH_{abs} is the heat of absorption from CO_2, and ΔH_{vap} is the heat of vaporization from MEA and water. The interfacial heat transfer, q_e, is dependent on the estimated heat transfer coefficient, h_e. It is assumed that the gas-side heat transfer is the controlling resistance in heat transfer between the gas and liquid phases for absorption. By using an enthalpy balance in the algorithm rather than fluid temperatures, T_V and T_L, a generalized set of equations may be established that are linked to a submodule that defines the enthalpy for the specific solvent of interest (e.g., aqueous MEA).

2.3. Correlations and Enhancement Factor Models. The mass transfer coefficients and interfacial area correlations used in the model here are derived from recent work by Rochelle and co-workers studying structured packing.[33−35] A benefit of these recent correlations is the reliance on only the geometric properties of the structured packing to estimate the effective interfacial area and mass transfer coefficients. Other correlations exist that have shown to be accurate but require measurements to determine packing-specific constants.[17,48,49] As the mass transfer coefficients for additively manufactured packing have not yet been determined, the correlations from Rochelle allow estimation of structured packing mass transfer properties for developing a deterministic absorption model. While other correlations for random, dumped packings exist for predicting mass transfer, only structured packing correlations are considered here in validating the modeling framework as the intensified device is composed of structured packing material for mass transfer.

The effective interfacial area, a_e, is estimated by[34]

$$\frac{a_e}{a_p} = 1.41\left[\left(\frac{\rho_L}{\sigma}\right)g^{1/3}\left(\frac{u_L}{a_p}\right)^{4/3}\right]^{0.116} \tag{12}$$

where a_p is the volume-specific packing area, ρ_L is the liquid-phase density, σ is the solvent surface tension, g is the gravity constant, and u_L is the superficial velocity of the liquid. The gas- and liquid-side mass transfer coefficients are determined by[35]

$$Sh_G = \frac{k_{g,i}}{a_p D_{g,i}} = 0.28 Sc_G^{0.5} Re_G^{0.62}\left(\frac{\sin 2\alpha_p}{\sin 2 \times 45°}\right)^{0.65} \tag{13a}$$

$$Sh_L = \frac{k_{l,i}}{a_p D_{l,i}} = 0.12 Sc_L^{0.5} Re_L^{0.565} Ga_L^{1/6}\left(\frac{Z}{1.8}\right)^{-0.54} \tag{13b}$$

where Sh is the Sherwood number, Sc is the Schmidt number, Re is the Reynolds number, Ga is the Galilei number, α_p is the corrugation angle of the structured packing, and Z is the height of the packing element.

The termolecular reaction mechanism between CO_2 and MEA is assumed to describe the reaction kinetics utilized in the Enhancement factor model. Aboudheir et al. previously studied a wide range of MEA concentrations, CO_2 loadings, and temperatures to determine the reaction rate equations for the termolecular mechanism[10]

$$-r_{CO_2} = (k_{MEA}[MEA]^2 + k_W[MEA][H_2O])[CO_2] = k_{app}[CO_2] \tag{14}$$

where k_{MEA} and k_W may be described by Arrhenius-type equations:

$$k_{MEA}\left(\frac{m^6}{kmol^2 s}\right) = 4.61e9\ \exp\left(\frac{-4412}{T}\right) \tag{15a}$$

$$k_W\left(\frac{m^6}{kmol^2 s}\right) = 4.55e6\ \exp\left(\frac{-3287}{T}\right) \tag{15b}$$

This kinetic model was developed by examining experimental kinetics data from a laminar jet absorber using highly-CO_2 loaded and highly concentrated MEA solutions. The free concentrations for MEA and H_2O in the rate model were calculated by chemical and vapor−liquid equilibria relationships using the same correlations from Edwards et al. and Kent and Eisenberg that are used in the model framework here. Recently, Amirkhosrow et al. utilized this kinetic model in predicting CO_2 capture pilot plant data and found it as the best performing kinetic model compared to other termolecular-based models.[50]

The model here first assumes that the Hatta number may be used directly as the Enhancement factor, E, designated as Model 1. The Hatta number, Ha, may be calculated by utilizing a combined apparent reaction rate of pseudo-first-order

$$Ha = \frac{\sqrt{D_{CO_2}k_{app}}}{k_{l,CO_2}} \tag{16}$$

where D_{CO_2} is the diffusion coefficient of CO_2 in aqueous MEA, and k_{app} is defined in eq 14. There are several other relationships for calculating the Enhancement factor. Putta et al. evaluated these models using available lab-scale CO_2 absorption data and provided a thorough discussion.[51]

Simulations with the Enhancement factor equivalent to the Hatta number are compared with another Enhancement factor model that incorporates equilibrium of the carbamate reaction into the Enhancement factor. The Enhancement factor for an instantaneous reaction with partially loaded MEA may be defined from Danckwerts and from Weiland[52,53]

$$E_\infty = 1 + \frac{\frac{D_{MEACOO^-}}{D_{CO_2}}\sqrt{K_{eq}}[MEA]}{\left[\left(1 + 2\frac{D_{MEACOO^-}}{D_{MEA}}\right)\sqrt{K_{eq}[CO_2]_i}\left(\sqrt{[CO_2]_b} + \sqrt{[CO_2]_i}\right)\right]} \tag{17a}$$

$$K_{eq} = \frac{[MEAH^+][MEACOO^-]}{[CO_2][MEA]^2} \tag{17b}$$

https://doi.org/10.1021/acs.iecr.1c02756
Ind. Eng. Chem. Res. 2021, 60, 14845−14855

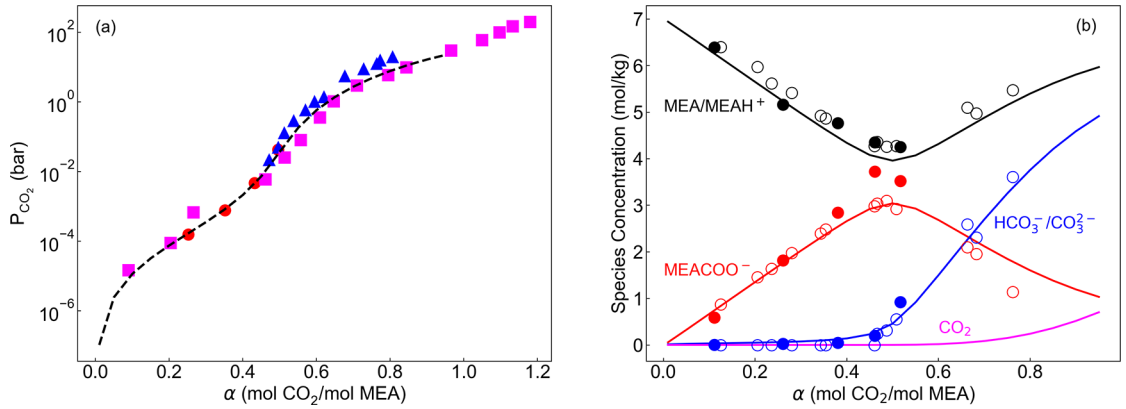

Figure 2. (a) Prediction (dashed black line) of CO_2 equilibrium pressure, P_{CO_2}, based on CO_2 loading, α, compared with literature data from Jou et al.[59] (magenta squares), Shen et al.[60] (blue triangles), and Dugas et al.[11] (red circles). (b) Prediction (lines) of chemical speciation based on CO_2 loading, α, compared with literature data from Hilliard[47] (solid symbols) and from Böttinger et al.[61] (empty symbols). T = 40 °C.

where K_{eq} represents the equilibrium constant for the termolecular reaction determined by the chemical equilibria of the reaction constants, K_1−K_5, D_i is the diffusivity in aqueous MEA for components $MEACOO^-$, MEA, and CO_2, and CO_2 concentrations for the bulk, b, and for the interface, i. This instantaneous Enhancement factor, E_∞, may then be used to estimate the Enhancement factor based on the expression from Wellek:[54]

$$E = 1 + \frac{1}{\left[\frac{1}{(E_\infty - 1)^{1.35}} + \frac{1}{(Ha - 1)^{1.35}}\right]^{1/1.35}} \tag{18}$$

Previous work has shown this Enhancement factor model to reliably predict packed bed absorber performance for reactions between CO_2 and MEA.[55,56] Use of this Enhancement factor is designated as Model 2.

2.4. Additively Manufactured Structured Packing.

Previous work by Miramontes et al. and Bolton et al. demonstrated the ability to incorporate coolant channels between corrugated structured packing sheets through additive manufacturing.[30−32] Both acrylonitrile butadiene styrene (ABS) plastic and aluminum materials were used for printing device-scale packing elements.[30,31] These studies focused on the experimental improvement in CO_2 capture observed from intrastage cooling within a structured packing device using aqueous MEA. A schematic in Figure 1b shows how the coolant flows countercurrent to the downflowing liquid solvent. Here, the aim is to develop a modeling framework that may be deterministic in predicting the CO_2 capture behavior in additively manufactured devices for CO_2 capture and potentially for other process modeling needs related to combined heat and mass transfer applications.

The energy balance equations presented in eqs 11a−11c represent an assumption of adiabatic behavior within a packing element stage. With the incorporation of an additively manufactured device that contains corrugated sheets for mass transfer and internal coolant channels for heat transfer, an additional heat flux equation for the liquid-phase and the enthalpy balance of the coolant are required to describe this packing section

$$H_{L,j+1}L_{j+1} - H_{L,j}L_j + q_c + q_e + \Delta H_{abs}N_{CO_2,j} + \sum_{i=MEA,W} \Delta H_{vap,i}N_{i,j} = 0 \tag{19a}$$

$$H_{c,j-1}L_{c,j-1} - H_{c,j}L_{c,j} - q_c = 0 \tag{19b}$$

$$q_c = h_{c,j}a_{e,j}A_j(T_{c,j} - T_{L,j})\Delta z \tag{19c}$$

where q_c is the coolant heat flux between the liquid phase and coolant, h_c is the heat transfer coefficient for the coolant, and T_c is the coolant temperature. From Miramontes et al., the overall heat transfer coefficient, U, is reported based on temperature measurements and log-mean temperature difference (LMTD) between the coolant and the absorption column. While an overall heat transfer coefficient based on experimental measurements may be used for process simulations, correlations for predicting the heat transfer coefficient may also be utilized to predict the CO_2 capture performance improvement in additively manufactured devices. The Nusselt number for laminar flow and a flat plate, which the liquid phase in solvent-based CO_2 capture absorption columns generally follows, may be calculated by the Chilton-Colburn analogy[57]

$$Nu = \frac{h_c}{\lambda_L a_p} = 0.332 Re_L^{1/2} Pr_L^{1/3} \tag{20}$$

where h_c is the coolant heat transfer coefficient, λ_L is the thermal conductivity of the solvent, and Pr_L is the liquid-phase Prandtl number. Simulations using the heat transfer coefficient estimated from eq 20 were compared with experimental CO_2 capture and axial temperature profile data to determine if correlations may be used to predict heat transfer performance within an additively manufactured device. The flat plate correlation is used here, but the geometry of the packing is composed of corrugated sheets. Therefore, the friction may vary for actual structured packing compared to flat plates, but eq 20 may be used as a first approximation to estimate the heat transfer coefficient.[57]

3. MODEL VALIDATION

The model framework relies on simplified chemical and vapor−liquid equilibria (VLE) relationships compared to other thermodynamic frameworks, such as electrolyte nonrandom two-liquid- (e-NRTL) or Pitzer-based activity coefficient models.[47,58] The equilibrium pressure data for CO_2 from solubility studies in aqueous MEA were compared with the VLE framework here. Figure 2a shows the predicted equilibrium pressure, P_{CO_2}, in relation to the CO_2 loading in

https://doi.org/10.1021/acs.iecr.1c02756
Ind. Eng. Chem. Res. 2021, 60, 14845−14855

Table 1. Summary of Absorption Column Pilot Plant Data Utilized in Modeling Framework Validation for Model 1 and Model 2[18,37]

case no.	G (kg/h)	L/G (mass:mass)	$y_{CO_2,f}$ (mol %)	α_{LEAN} (mol CO_2/mol MEA)	reported CO_2 capture (%)	model 1 simulated CO_2 capture (%)	model 2 simulated CO_2 capture (%)
				Morgan et al.			
K13	2238	3.0	9.35	0.164	97.98	99.75	99.66
K17	2240	3.0	9.19	0.168	97.61	99.62	99.47
K18	2271	3.0	10.19	0.141	92.85	99.22	97.63
K19	1440	8.2	11.00	0.184	98.21	99.81	99.71
K20	1324	2.4	10.98	0.075	95.55	99.85	98.64
K21	1366	2.3	10.18	0.074	96.32	99.93	99.91
				Zhang et al.			
13	952	3.8	16.8	0.33	62	71.3	61.1
19	424	4.2	17.0	0.27	95	97.5	89.8
20	424	3.4	17.0	0.27	87	85.2	76.2
22	424	3.0	17.3	0.28	72	73.3	65.4
24	668	3.7	15.2	0.28	92	92.7	83.5

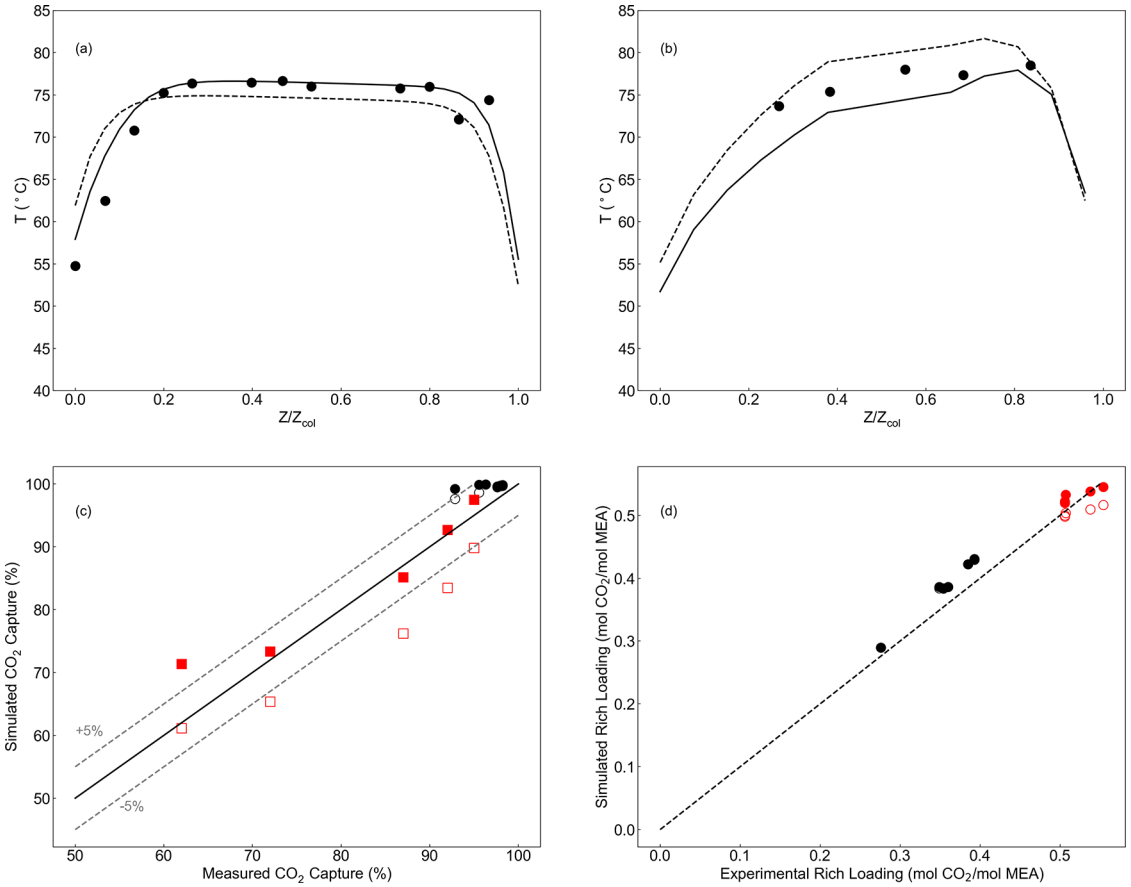

Figure 3. (a) Axial temperature profile for Case K13 from Morgan et al.[18] (symbols) compared with Model 1 (dashed line) and Model 2 (solid line). (b) Axial temperature profile for Case 19 from Zhang et al.[37] (symbols) compared with Model 1 (dashed line) and Model 2 (solid line). (c) Parity plot for CO_2 capture for all cases summarized in Table 1 from Morgan et al. (black circle symbols; closed − Model 1; open − Model 2) and Zhang et al. (red square symbols; closed − Model 1; open − Model 2). Solid and dashed lines represent parity and ±5%, respectively. (d) Parity plot for rich CO_2 loading in solvent for all cases summarized in Table 1 from Morgan et al. (black circle symbols; closed − Model 1; open − Model 2) and Zhang et al. (red square symbols; closed − Model 1; open − Model 2). Dashed line represents parity.

the solvent, α, compared with data from three published sources using 30 wt % MEA solutions at 40 °C.[11,59,60] There is good agreement between these data and the VLE prediction, especially in the CO_2 loading range below 0.5, where absorption columns primarily operate for CO_2 capture. These VLE predictions are also consistent with Aboudheir et al., who observed good agreement with published solubility data using the same equilibria relationships.[10] Figure 2b compares nuclear magnetic resonance (NMR) speciation data from Hilliard and from Böttinger et al. with ionic species predicted by the chemical equilibria in the VLE model framework.[47,61] Both the NMR data and the speciation prediction show an increase in the carbamate concentration up to a CO_2 loading of 0.5 and then a subsequent decrease in

https://doi.org/10.1021/acs.iecr.1c02756
Ind. Eng. Chem. Res. 2021, 60, 14845−14855

its concentration with increasing concentration for other dissolved CO_2 species (e,g., HCO_3^-, CO_3^-, and CO_2). The species for MEA and $MEAH^+$ were combined in both studies, as these two are difficult to separately determine using NMR techniques.[47] While speciation predicted by the model framework for the absorbed CO_2, $MEACOO^-$, and HCO_3^-/CO_3^{2-} agrees well with these published data, there is slight underprediction of the MEA/$MEAH^+$ concentration in solution. This observation suggests that, in modeling absorption and stripping columns, the Enhancement factor may be lower if the model predicts less free amine available for reaction. Comparisons between available CO_2 solubility data and NMR speciation at other temperatures are provided in the Supporting Information.

Pilot plant data for the absorption column from Morgan et al. and Zhang et al. were used to compare validity of the Enhancement factor models, Model 1 and Model 2, to predict CO_2 capture using aqueous MEA solutions.[18,37] The absorption column conditions for these CO_2 capture data are summarized in Table 1. The cases selected here represent adiabatic conditions from both studies to benchmark the model framework prior to simulating intrastage cooling using additively manufactured packing. There were additional cases from both pilot plant studies that are not considered here. In Morgan et al., other cases included interstage cooling between packed bed sections of the absorption column. These cases may be considered in a later study that would compare the effectiveness of interstage cooling using traditional heat exchangers and pump around process schemes and the effectiveness of intrastage cooling with an additively manufactured structured packing device. Other cases in Zhang et al. were excluded as they had similar liquid-to-gas ratios and lean CO_2 loadings as the cases already considered from Morgan et al. Only cases with higher lean CO_2 loadings were considered here to understand the validity of the model framework across a wide range of process conditions.

Morgan et al. previously used these pilot plant data to develop a rigorous, rate-based model using Aspen Plus with a custom Fortran-linked library to implement models not available in the commercial software and to quantify the uncertainty for predicting CO_2 capture, temperature bulge in the column, and associated solvent regeneration for the stripping column reboiler.[17,18] All cases from Morgan et al. that operated under adiabatic conditions achieved greater than 90% CO_2 capture within a narrow range of both the CO_2 lean loading in the MEA solvent and the CO_2 feed mole fraction in the flue gas stream. The structured packing used for these cases was Mellapak 252Y from Sulzer, which has similar geometric properties as Mellapak 250Y packing and the additively manufactured structured packing devices that were used in Miramontes et al.[18,32]

Zhang et al. utilized the pilot plant data in their study to also validate a rate-based model for aqueous MEA solutions using Aspen Plus.[37] They demonstrated the range of simulation results obtained when using different rate-based models within the Aspen Plus RateSep model library and superior prediction in pilot plant results when compared to equilibrium-based models. These simulations were able to predict the CO_2 loading in the rich solvent, the CO_2 capture rate, and temperature profile for a wide range of CO_2 lean loadings and solvent-to-gas ratios. The packing used in this study was Flexipac 1Y from Koch-Glisch, which will aid in demonstrating how effective the model framework is in predicting CO_2 capture in various structured packing geometries.

The simulation results for both Enhancement factor models, Model 1 and Model 2, are summarized in both Table 1 and Figure 3. The model framework and Enhancement factor models were assessed based on accuracy in predicting CO_2 capture in the absorption column, the temperature bulge within the column, and the CO_2 loading in the rich solvent. These data were reported in the pilot plant studies used for validating the model framework here and serve as the common basis of comparison for the Enhancement factor models and the absorption column pilot plant data. As shown in Table 1 for Model 1, which utilizes the Hatta number for the Enhancement factor, there is generally an overprediction in the CO_2 capture compared with the absorption column data. However, the average relative deviation (ARD) for CO_2 capture for all cases is 3.9% for Model 1, while the ARD for Model 2 is 5.0%. As shown in Figure 3c, a parity plot of reported CO_2 capture from these pilot studies was compared with the simulated CO_2 capture using the model framework; this is, in part, due to the underprediction in CO_2 capture for the pilot data from Zhang et al. when using Model 2 for the Enhancement factor in the simulations. While the relatively low ARD value suggests Model 1 may be able to predict the CO_2 capture in an absorption column as a first approximation, other factors should be considered, such as temperature rises associated with absorption and exiting solvent concentration from the column.

The incorporation of both the Hatta number and the instantaneous Enhancement factor generally led to better estimation of the temperature bulge in the absorption column when comparing the liquid-phase temperature predicted by Model 2 to temperature profile data from Morgan et al. In Figure 3a, the temperature profile data from case K13 (symbols) were consistently better predicted by Model 2 (solid line, liquid-phase temperature), and the simulation was able to predict the maximum temperature rise and position of the temperature bulge within the absorption column. Comparing other cases from Morgan et al. to temperature profiles from Model 2 showed consistency in improved prediction of the temperature increases in the absorption column. In Figure 3b, the temperature profile data from case 19 (symbols) of Zhang et al. are between the predictions of Model 1 (dashed line) and Model 2 (solid line). In this case from Zhang et al., the CO_2 capture is predicted more accurately by Model 1, but the temperature bulge for the liquid phase of Model 1 exceeds the reported pilot plant data. As suggested by Morgan et al., the uncertainty in the solvent composition, especially at higher lean CO_2 loadings, may strongly influence how well a model may estimate the CO_2 capture and temperature profile within an absorption column.[18] These uncertainties may influence how well the simulations here predict these data from Zhang et al. The rich CO_2 loading in the solvent predicted by both models is shown in Figure 3d as a parity plot against the reported rich CO_2 loadings.[18,37] The observed differences in the rich loadings between Model 1 and Model 2 are correlated with the difference in CO_2 capture observed between the two models; however, the ARD values for the rich CO_2 loading for Model 1 and Model 2 were 5.7% and 5.9%, respectively. This suggests either Enhancement factor model does not strongly influence the overall solvent composition in the rich solvent stream. Overall, these simulation results demonstrate the capability of

https://doi.org/10.1021/acs.iecr.1c02756
Ind. Eng. Chem. Res. 2021, 60, 14845−14855

Table 2. Summary of Adiabatic and Intrastage Cooling Conditions from Miramontes et al. and Predicted Lean CO_2 Loadings from Model 1 and Model 2

case no.	G (kg/h)	L/G(mass:mass)	$y_{CO_2,f}$ (mol %)	CO_2 capture adiabatic (%)	CO_2 capture cooling (%)	$\alpha_{LEAN,1}$ (mol CO_2/mol MEA)	$\alpha_{LEAN,2}$ (mol CO_2/mol MEA)
M1	38.4	5.2	20	78	88	0.311	0.289
M2	32.5	6.2	10	83	87	0.361	0.351
M3	35.3	5.7	15	58	67	0.398	0.383
M4	41.9	4.8	25	62	66	0.318	0.294
M5	73.1	2.8	10	60	61	0.349	0.329
M6	50.0	4.0	15	73	77	0.320	0.299
M7	38.4	5.2	20	78	88	0.311	0.289
M8	31.0	6.5	25	94	98	0.261	0.236

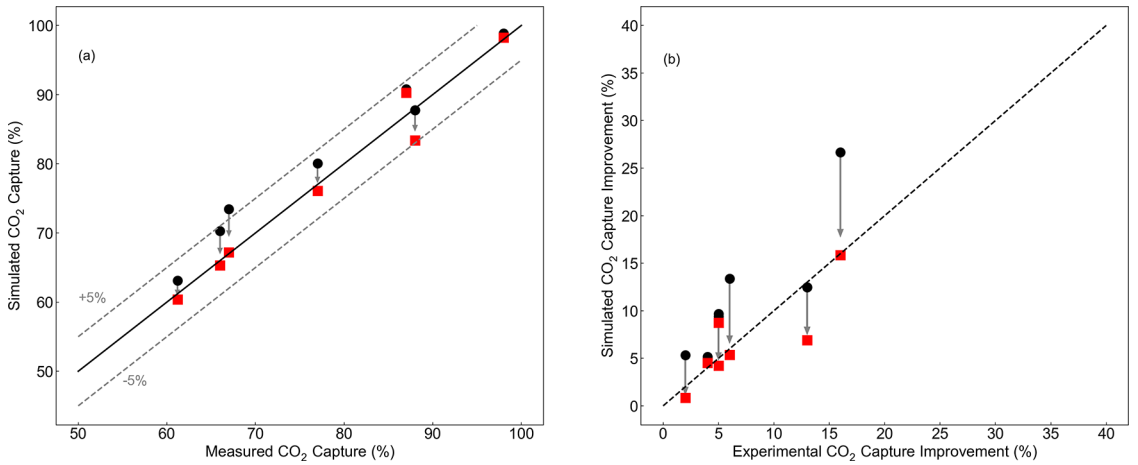

Figure 4. Parity plots for CO_2 capture with intrastage cooling (a) and CO_2 capture improvement over adiabatic operation (b). Black circles: Model 1; red squares: Model 2. Arrows indicate direction of change for simulation results from Model 1 to Model 2. Most cases showed reduction in CO_2 capture improvement when comparing Model 1 to Model 2.

the model framework presented here to estimate the CO_2 capture performance across a wide range of operating conditions, column scales, and structured packing.

4. RATE-BASED MODELING WITH ADDITIVELY MANUFACTURED STRUCTURED PACKING

To predict the CO_2 capture performance from intrastage cooling and its improvement over adiabatic operation using the rate-based model framework and to compare with data from Miramontes et al., the lean CO_2 loading in the solvent was estimated by matching the CO_2 capture performance in the adiabatic bench-scale conditions. This was performed by using an objective function within the Pyomo modeling language and allowing the lean CO_2 loading in the solvent to change for the adiabatic simulation to match the experimental data. This approach was used because the CO_2 concentration in the lean solvent was not measured by Miramontes et al.[32] Once this lean loading was determined from adiabatic conditions, the lean loading in the solvent was fixed to this value to predict the CO_2 capture for intrastage cooling based on the experimental conditions summarized in Table 2. This modeling approach is consistent with the experimental procedure followed by Miramontes et al.

All lean CO_2 loadings were predicted to be greater than 0.2 mol CO_2/mol MEA, which correspond closer to the lean solvent loadings for pilot plant data in Zhang et al. As Model 2 incorporates an instantaneous Enhancement factor and equilibrium constant in the modeling framework, there is lower predicted lean CO_2 loading in the solvent compared with Model 1. This is consistent with a lower Enhancement factor predicted by Model 2, which would require a larger driving force (e.g., less CO_2 in the lean solvent) for mass transfer to reach an equivalent CO_2 capture at the conditions summarized in Table 2. A 10% relative difference or less in the lean CO_2 loading between the two Enhancement factor models is observed in Table 2.

The CO_2 capture prediction and the improvement in capture from intrastage cooling are summarized in Figure 4 for both models. The parity plot for CO_2 capture, Figure 4a, demonstrates an overprediction of the CO_2 capture with intrastage cooling when Model 1 is used as the Enhancement factor. Simulations that utilized Model 2 all show a decrease in the predicted CO_2 capture relative to Model 1 simulations, ranging from 1 to 5% reduction in the capture rate. Apart from case M1, the capture rate improvement with cooling observed with Model 2 more closely represents the reported CO_2 capture from Miramontes et al. The ARD for CO_2 capture from Model 1 and Model 2 is 3.6% and 2.3%, respectively. Another method of assessing the deterministic nature of these rate-based models is to compare the CO_2 capture improvement for each case as shown in Figure 4b. In all cases, there is a decrease in the improvement predicted by Model 2 relative to Model 1 simulations. The largest decrease in capture improvement was observed for case M3, reducing from 25% using Model 1 to 15% using Model 2. Overall, these simulation results suggest Model 2 may more accurately predict the observed CO_2 capture in these bench-scale data. This is consistent with the model validation of the modeling

https://doi.org/10.1021/acs.iecr.1c02756
Ind. Eng. Chem. Res. 2021, 60, 14845−14855

framework when comparing simulation results with absorption column pilot plant data from Morgan et al. and Zhang et al.

To understand the relative ability for predicting the heat transfer from the absorption column to the coolant and enthalpy balance of intrastage cooling devices, the temperature profile from Miramontes et al., case M1 (symbols), in Figure 5

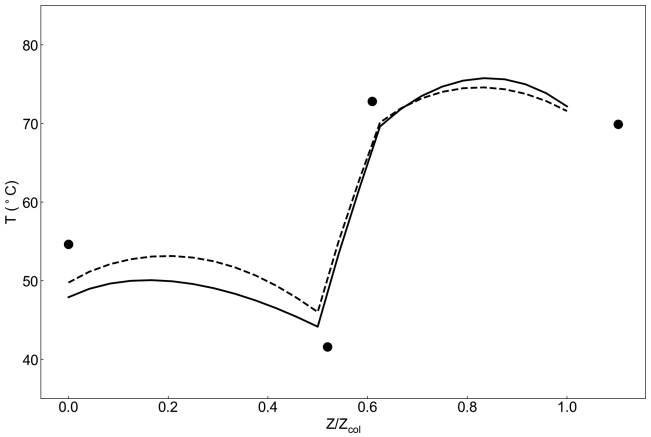

Figure 5. Temperature profile with intrastage cooling of Case M1 (symbols) compared with prediction using Model 1 (dashed line) and Model 2 (solid line).

was compared with both Model 1 (dashed line) and Model 2 (solid line). In both models, there is a correlated decrease in the temperature in the axial position of the intrastage cooling device. The liquid-phase temperature at the inlet to the additively manufactured device at approximately 0.6 Z/Z_{col} was 2 °C less than the reported temperature, while the liquid-phase temperature for the outlet of the device was between 2 and 5 °C higher. This suggests that the correlation based on the Chilton-Colburn analogy using the liquid-phase Reynolds and Prandtl numbers may be sufficient for estimating the heat transfer properties of the additively manufactured device. Based on the relationship in eq 20, the properties which influence the observed heat transfer coefficient would then be related to the properties of the solvent and the geometric surface area of the packing. Further study examining the effect of these properties with different solvents and geometric structured packing parameters may reveal if the correlation utilized here would be accurate in predicting the heat transfer phenomena in the packing.

5. CONCLUSIONS

A rate-based absorption model framework using Enhancement factor models has been validated based on previously published absorption column pilot plant data from two separate sources at different column scales and packing geometries. This wide applicability is due, in part, to the recent development of mass transfer correlations for structured packing and its implementation in the rate-based model framework presented here. This framework was applied toward predicting the effect of additively manufactured structured packing on the improvement of CO_2 capture. These simulation results demonstrate the model framework proposed here may be applied in estimating the CO_2 capture, temperature profile, and solvent composition for aqueous MEA-based absorption systems that utilize these 3D-printed structured packing devices as well as commercial structured packing. The main advantage of this model framework is that new structured packing devices may be designed, and performance of new packing geometries may be estimated using mass transfer and heat transfer relationships validated here without extensive testing campaigns. This may enhance the prototyping and speed up the development of this new type of structured packing. Other research areas would be to investigate the model framework for its application toward other solvent systems for CO_2 capture as next-generation solvents are further developed and to validate the modeling framework with stripping columns for an integrated process model.

■ ASSOCIATED CONTENT

Supporting Information

The Supporting Information is available free of charge at https://pubs.acs.org/doi/10.1021/acs.iecr.1c02756.

Table of equations used in model framework and comparison of modeling framework and published CO_2 solubility and NMR speciation data at 25, 60, and 80 °C (PDF)

■ AUTHOR INFORMATION

Corresponding Author

Joshua A. Thompson − *Manufacturing Science Division, Oak Ridge National Laboratory, Oak Ridge, Tennessee 37830, United States;* orcid.org/0000-0002-8035-0558; Email: thompsonja@ornl.gov

Author

Costas Tsouris − *Manufacturing Science Division, Oak Ridge National Laboratory, Oak Ridge, Tennessee 37830, United States;* orcid.org/0000-0002-0522-1027

Complete contact information is available at: https://pubs.acs.org/10.1021/acs.iecr.1c02756

Notes

The authors declare no competing financial interest.

Biography

Dr. Joshua A. Thompson has a B.ChE. from the Department of Chemical Engineering at Auburn University and a Ph.D. from the Department of Chemical & Biomolecular Engineering at Georgia Institute of Technology. He has 7 years of industry experience working at Chevron Corporation in the areas of adsorption, absorption, and mercury capture, where he was an inventor of 12 patents and patent applications and author of 5 journal articles. He is now working as a Research Scientist at Oak Ridge National Laboratory in the Chemical Process Scale-Up Group, focused on carbon capture and energy-related separations.

■ ACKNOWLEDGMENTS

This research was funded by the Office of Fossil Energy of the U.S. Department of Energy under Contract DE-AC05-00OR22725. This invited contribution is part of the I&EC Research special issue for the 2021 Class of Influential Researchers.

■ REFERENCES

(1) Aaron, D.; Tsouris, C. Separation of CO_2 from Flue Gas: A Review. *Sep. Sci. Technol.* **2005**, *40* (1−3), 321−348.
(2) Cebrucean, D.; Cebrucean, V.; Ionel, I. CO_2 Capture and Storage from Fossil Fuel Power Plants. *Energy Procedia* **2014**, *63*, 18−26.
(3) Jansen, D.; Gazzani, M.; Manzolini, G.; Dijk, E. v.; Carbo, M. Pre-combustion CO_2 capture. *Int. J. Greenhouse Gas Control* **2015**, *40*, 167−187.
(4) Nemitallah, M. A.; Habib, M. A.; Badr, H. M.; Said, S. A.; Jamal, A.; Ben-Mansour, R.; Mokheimer, E. M. A.; Mezghani, K. Oxy-fuel combustion technology: current status, applications, and trends. *Int. J. Energy Res.* **2017**, *41* (12), 1670−1708.
(5) Sanz-Perez, E. S.; Murdock, C. R.; Didas, S. A.; Jones, C. W. Direct Capture of CO_2 from Ambient Air. *Chem. Rev.* **2016**, *116* (19), 11840−11876.
(6) Wang, M.; Lawal, A.; Stephenson, P.; Sidders, J.; Ramshaw, C. Post-combustion CO_2 capture with chemical absorption: A state-of-the-art review. *Chem. Eng. Res. Des.* **2011**, *89* (9), 1609−1624.
(7) Samanta, A.; Zhao, A.; Shimizu, G. K. H.; Sarkar, P.; Gupta, R. Post-Combustion CO_2 Capture Using Solid Sorbents: A Review. *Ind. Eng. Chem. Res.* **2012**, *51* (4), 1438−1463.
(8) Wang, Y.; Zhao, L.; Otto, A.; Robinius, M.; Stolten, D. A Review of Post-combustion CO_2 Capture Technologies from Coal-fired Power Plants. *Energy Procedia* **2017**, *114*, 650−665.
(9) Rochelle, G. T. Amine scrubbing for CO_2 capture. *Science* **2009**, *325* (5948), 1652−4.
(10) Aboudheir, A.; Tontiwachwuthikul, P.; Chakma, A.; Idem, R. Kinetics of the reactive absorption of carbon dioxide in high CO_2-loaded, concentrated aqueous monoethanolamine solutions. *Chem. Eng. Sci.* **2003**, *58* (23−24), 5195−5210.
(11) Dugas, R.; Rochelle, G. Absorption and desorption rates of carbon dioxide with monoethanolamine and piperazine. *Energy Procedia* **2009**, *1* (1), 1163−1169.
(12) Mobley, P. D.; Rayer, A. V.; Tanthana, J.; Gohndrone, T. R.; Soukri, M.; Coleman, L. J. I.; Lail, M. CO_2 Capture Using Fluorinated Hydrophobic Solvents. *Ind. Eng. Chem. Res.* **2017**, *56* (41), 11958−11966.
(13) Seo, K.; Tsay, C.; Hong, B.; Edgar, T. F.; Stadtherr, M. A.; Baldea, M. Rate-Based Process Optimization and Sensitivity Analysis for Ionic-Liquid-Based Post-Combustion Carbon Capture. *ACS Sustainable Chem. Eng.* **2020**, *8* (27), 10242−10258.
(14) Notz, R.; Tönnies, I.; Mangalapally, H. P.; Hoch, S.; Hasse, H. A short-cut method for assessing absorbents for post-combustion carbon dioxide capture. *Int. J. Greenhouse Gas Control* **2011**, *5* (3), 413−421.
(15) Plaza, J. M.; Wagener, D. V.; Rochelle, G. T. Modeling CO_2 capture with aqueous monoethanolamine. *Energy Procedia* **2009**, *1* (1), 1171−1178.
(16) Rayer, A. V.; Mobley, P. D.; Soukri, M.; Gohndrone, T. R.; Tanthana, J.; Zhou, J.; Lail, M. Absorption rates of carbon dioxide in amines in hydrophilic and hydrophobic solvents. *Chem. Eng. J.* **2018**, *348*, 514−525.
(17) Soares Chinen, A.; Morgan, J. C.; Omell, B.; Bhattacharyya, D.; Tong, C.; Miller, D. C. Development of a Rigorous Modeling Framework for Solvent-Based CO_2 Capture. 1. Hydraulic and Mass Transfer Models and Their Uncertainty Quantification. *Ind. Eng. Chem. Res.* **2018**, *57* (31), 10448−10463.
(18) Morgan, J. C.; Soares Chinen, A.; Omell, B.; Bhattacharyya, D.; Tong, C.; Miller, D. C.; Buschle, B.; Lucquiaud, M. Development of a Rigorous Modeling Framework for Solvent-Based CO_2 Capture. Part 2: Steady-State Validation and Uncertainty Quantification with Pilot Plant Data. *Ind. Eng. Chem. Res.* **2018**, *57* (31), 10464−10481.
(19) Zhou, S. J.; Tanthana, J.; Mobley, P.; Rayer, A. V.; Gupta, V.; Lesemann, M.; Soukri, M.; Lail, M.; Tobiesen, A.; Mejdell, T.; Aronu, U. E.; Grimstvedt, A.; Hjarbo, K.; Hovdahl, L. Pilot Testing of a Non-Aqueous Solvent (NAS) CO_2 Capture Process. *14th Greenhouse Gas Control Technologies Conference (GHGT-14), Melbourne, 21−26 October 2018*; Melbourne, 2018.
(20) Tanthana, J.; Rayer, A. V.; Gupta, V.; Mobley, P. D.; Soukri, M.; Zhou, J.; Lail, M. Experimental Study of a Hydrophobic Solvent for Natural Gas Sweetening Based on the Solubility and Selectivity for Light Hydrocarbons (CH_4, C_2H_6) and Acid Gases (CO_2 and H_2S) at 298−353 K. *J. Chem. Eng. Data* **2019**, *64* (2), 545−556.
(21) Gao, T.; Selinger, J. L.; Rochelle, G. T. Demonstration of 99% CO_2 removal from coal flue gas by amine scrubbing. *Int. J. Greenhouse Gas Control* **2019**, *83*, 236−244.
(22) Gao, T.; Rochelle, G. T. CO_2 Absorption from Gas Turbine Flue Gas by Aqueous Piperazine with Intercooling. *Ind. Eng. Chem. Res.* **2020**, *59* (15), 7174−7181.
(23) Tobiesen, F. A.; Svendsen, H. F.; Juliussen, O. Experimental validation of a rigorous absorber model for CO_2 postcombustion capture. *AIChE J.* **2007**, *53* (4), 846−865.
(24) Rochelle, G.; Chen, E.; Freeman, S.; Van Wagener, D.; Xu, Q.; Voice, A. Aqueous piperazine as the new standard for CO_2 capture technology. *Chem. Eng. J.* **2011**, *171* (3), 725−733.
(25) Tsay, C.; Pattison, R. C.; Zhang, Y.; Rochelle, G. T.; Baldea, M. Rate-based modeling and economic optimization of next-generation amine-based carbon capture plants. *Appl. Energy* **2019**, *252*, 113379.
(26) Zhang, Y.; Sachde, D.; Chen, E.; Rochelle, G. Modeling of absorber pilot plant performance for CO_2 capture with aqueous piperazine. *Int. J. Greenhouse Gas Control* **2017**, *64*, 300−313.
(27) Reay, D. The role of process intensification in cutting greenhouse gas emissions. *Appl. Therm. Eng.* **2008**, *28* (16), 2011−2019.
(28) Wang, M.; Joel, A. S.; Ramshaw, C.; Eimer, D.; Musa, N. M. Process intensification for post-combustion CO_2 capture with chemical absorption: A critical review. *Appl. Energy* **2015**, *158*, 275−291.
(29) Jang, G. G.; Thompson, J. A.; Sun, X.; Tsouris, C. Process intensification of CO_2 capture by low-aqueous solvent. *Chem. Eng. J.* **2021**, *426*, 131240.
(30) Bolton, S.; Kasturi, A.; Palko, S.; Lai, C.; Love, L.; Parks, J.; Xin, S.; Tsouris, C. 3D printed structures for optimized carbon capture technology in packed bed columns. *Sep. Sci. Technol.* **2019**, *54* (13), 2047−2058.
(31) Miramontes, E.; Love, L. J.; Lai, C.; Sun, X.; Tsouris, C. Additively manufactured packed bed device for process intensification of CO2 absorption and other chemical processes. *Chem. Eng. J.* **2020**, *388*, 124092.
(32) Miramontes, E.; Jiang, E. A.; Love, L. J.; Lai, C.; Sun, X.; Tsouris, C. Process intensification of CO_2 absorption using a 3D printed intensified packing device. *AIChE J.* **2020**, *66* (8), e16285.
(33) Wang, C.; Perry, M.; Seibert, F.; Rochelle, G. Packing Characterization for Post Combustion CO_2 Capture: Mass Transfer Model Development. *Energy Procedia* **2014**, *63*, 1727−1744.
(34) Wang, C.; Song, D.; Seibert, F. A.; Rochelle, G. T. Dimensionless Models for Predicting the Effective Area, Liquid-Film, and Gas-Film Mass-Transfer Coefficients of Packing. *Ind. Eng. Chem. Res.* **2016**, *55* (18), 5373−5384.
(35) Song, D.; Seibert, A. F.; Rochelle, G. T. Mass Transfer Parameters for Packings: Effect of Viscosity. *Ind. Eng. Chem. Res.* **2018**, *57* (2), 718−729.
(36) Akula, P.; Eslick, J.; Bhattacharyya, D.; Miller, D. C. Model Development, Validation, and Optimization of an MEA-Based Post-Combustion CO_2 Capture Process under Part-Load and Variable Capture Operations. *Ind. Eng. Chem. Res.* **2021**, *60* (14), 5176−5193.
(37) Zhang, Y.; Chen, H.; Chen, C. C.; Plaza, J. M.; Dugas, R.; Rochelle, G. T. Rate-Based Process Modeling Study of CO_2 Capture

https://doi.org/10.1021/acs.iecr.1c02756
Ind. Eng. Chem. Res. 2021, 60, 14845−14855

with Aqueous Monoethanolamine Solution. *Ind. Eng. Chem. Res.* **2009**, *48* (20), 9233−9246.
(38) Saimpert, M.; Puxty, G.; Qureshi, S.; Wardhaugh, L.; Cousins, A. A new rate based absorber and desorber modelling tool. *Chem. Eng. Sci.* **2013**, *96*, 10−25.
(39) Higler, A.; Taylor, R.; Krishna, R. Modeling of a reactive separation process using a nonequilibrium stage model. *Comput. Chem. Eng.* **1998**, *22*, S111−S118.
(40) Baur, R.; Higler, A. P.; Taylor, R.; Krishna, R. Comparison of equilibrium stage and nonequilibrium stage models for reactive distillation. *Chem. Eng. J.* **2000**, *76* (1), 33−47.
(41) Hart, W. E.; Watson, J.-P.; Woodruff, D. L. Pyomo: modeling and solving mathematical programs in Python. *Math. Program. Comput.* **2011**, *3* (3), 219−260.
(42) Hart, W. E.; Laird, C.; Watson, J.-P.; Woodruff, D. L. *Pyomo − Optimization Modeling in Python*; Springer: 2012; 245pp, DOI: 10.1007/978-1-4614-3226-5.
(43) Wächter, A.; Biegler, L. T. On the implementation of an interior-point filter line-search algorithm for large-scale nonlinear programming. *Math. Program.* **2006**, *106* (1), 25−57.
(44) Edwards, T. J.; Maurer, G.; Newman, J.; Prausnitz, J. M. Vapor-liquid equilibria in multicomponent aqueous solutions of volatile weak electrolytes. *AIChE J.* **1978**, *24* (6), 966−976.
(45) Kent, R. L.; Eisenberg, B. Better Data for Amine Treating. *Hydrocarbon Processing* **1976**, *55* (2), 87−90.
(46) Wang, Y. W.; Xu, S.; Otto, F. D.; Mather, A. E. Solubility of N_2O in Alkanolamines and in Mixed-Solvents. *Chem. Eng. J.* **1992**, *48* (1), 31−40.
(47) Hilliard, M. D. *A Predictive Thermodynamic Model for an Aqueous Blend of Potassium Carbonate, Piperazine, and Monoethanolamine for Carbon Dioxide Capture from Flue Gas.* Ph.D. Thesis. The University of Texas at Austin, Austin, TX, 2008. http://hdl.handle.net/2152/3900 (accessed 2021-04-14).
(48) Billet, R.; Schultes, M. Predicting mass transfer in packed columns. *Chem. Eng. Technol.* **1993**, *16* (1), 1−9.
(49) Billet, R.; Schultes, M. Prediction of mass transfer columns with dumped and arranged packings - Updated summary of the calculation method of Billet and Schultes. *Chem. Eng. Res. Des.* **1999**, *77* (A6), 498−504.
(50) Amirkhosrow, M.; Pérez-Calvo, J.-F.; Gazzani, M.; Mazzotti, M.; Nemati Lay, E. Rigorous rate-based model for CO2 capture via monoethanolamine-based solutions: effect of kinetic models, mass transfer, and holdup correlations on prediction accuracy. *Sep. Sci. Technol.* **2021**, *56*, 1491.
(51) Putta, K. R.; Tobiesen, F. A.; Svendsen, H. F.; Knuutila, H. K. Applicability of enhancement factor models for CO2 absorption into aqueous MEA solutions. *Appl. Energy* **2017**, *206*, 765−783.
(52) Danckwerts, P. V. *Gas-Liquid Reactions.*; McGraw-Hill: New York, 1971.
(53) Weiland, R. H.; Rawal, M.; Rice, R. G. Stripping of carbon dioxide from monoethanolamine solutions in a packed column. *AIChE J.* **1982**, *28* (6), 963−973.
(54) Wellek, R. M.; Brunson, R. J.; Law, F. H. Enhancement factors for gas-absorption with second-order irreversible chemical reaction. *Can. J. Chem. Eng.* **1978**, *56* (2), 181−186.
(55) Tontiwachwuthikul, P.; Meisen, A.; Lim, C. J. CO_2 absorption by NaOH, monoethanolamine and 2-amino-2-methyl-1-propanol solutions in a packed column. *Chem. Eng. Sci.* **1992**, *47* (2), 381−390.
(56) Shahid, M. Z.; Maulud, A. S.; Bustam, M. A.; Suleman, H.; Halim, H. N. A.; Shariff, A. M. Rate-Based Modeling for Packed Absorption Column of the MEA−CO_2−Water System at High-Pressure and High-CO_2 Loading Conditions. *Ind. Eng. Chem. Res.* **2019**, *58* (27), 12235−12246.
(57) Chilton, T. H.; Colburn, A. P. Mass Transfer (Absorption) Coefficients Prediction from Data on Heat Transfer and Fluid Friction. *Ind. Eng. Chem.* **1934**, *26* (11), 1183−1187.
(58) Wagner, M.; von Harbou, I.; Kim, J.; Ermatchkova, I.; Maurer, G.; Hasse, H. Solubility of Carbon Dioxide in Aqueous Solutions of Monoethanolamine in the Low and High Gas Loading Regions. *J. Chem. Eng. Data* **2013**, *58* (4), 883−895.
(59) Jou, F.-Y.; Mather, A. E.; Otto, F. D. The solubility of CO_2 in a 30 mass percent monoethanolamine solution. *Can. J. Chem. Eng.* **1995**, *73* (1), 140−147.
(60) Shen, K. P.; Li, M. H. Solubility of carbon dioxide in aqueous mixtures of monoethanolamine with methyldiethanolamine. *J. Chem. Eng. Data* **1992**, *37* (1), 96−100.
(61) Böttinger, W.; Maiwald, M.; Hasse, H. Online NMR spectroscopic study of species distribution in MEA−H_2O−CO_2 and DEA−H_2O−CO_2. *Fluid Phase Equilib.* **2008**, *263* (2), 131−143.

https://doi.org/10.1021/acs.iecr.1c02756
Ind. Eng. Chem. Res. 2021, 60, 14845−14855